

A Near-Uniform Basin-Wide Sea Level Fluctuation of the Mediterranean Sea

ICHIRO FUKUMORI, DIMITRIS MENEMENLIS, AND TONG LEE

Jet Propulsion Laboratory, California Institute of Technology, Pasadena, California

(Manuscript received 3 May 2005, in final form 24 January 2006)

ABSTRACT

A new basin-wide oscillation of the Mediterranean Sea is identified and analyzed using sea level observations from the Ocean Topography Experiment (TOPEX)/Poseidon satellite altimeter and a numerical ocean circulation model. More than 50% of the large-scale, nontidal, and non-pressure-driven variance of sea level can be attributed to this oscillation, which is nearly uniform in phase and amplitude across the entire basin. The oscillation has periods ranging from 10 days to several years and has a magnitude as large as 10 cm. The model suggests that the fluctuations are driven by winds at the Strait of Gibraltar and its neighboring region, including the Alboran Sea and a part of the Atlantic Ocean immediately to the west of the strait. Winds in this region force a net mass flux through the Strait of Gibraltar to which the Mediterranean Sea adjusts almost uniformly across its entire basin with depth-independent pressure perturbations. The wind-driven response can be explained in part by wind setup; a near-stationary balance is established between the along-strait wind in this forcing region and the sea level difference between the Mediterranean Sea and the Atlantic Ocean. The amplitude of this basin-wide wind-driven sea level fluctuation is inversely proportional to the setup region's depth but is insensitive to its width including that of Gibraltar Strait. The wind-driven fluctuation is coherent with atmospheric pressure over the basin and contributes to the apparent deviation of the Mediterranean Sea from an inverse barometer response.

1. Introduction

The Mediterranean Sea, being a semienclosed basin, is often considered a test bed for studying ocean general circulation. Its relatively small size in comparison with the global ocean is conducive to synoptic observations [e.g., the Physical Oceanography of the Eastern Mediterranean program; POEM Group (1992)] and high-resolution numerical modeling (e.g., Korres et al. 2000).

Yet its basin-wide circulation cannot be considered in isolation. Exchange through the Strait of Gibraltar plays a critical role in regulating the circulation of the Mediterranean Sea and its outflow affects global ocean circulation [see, e.g., Candela (2001) for a recent review]. The Mediterranean Sea has an excess of evaporation over precipitation. Mass and salt budgets of the basin consequently require a net inflow through the Strait of Gibraltar, and a baroclinic exchange of out-

flowing salty Mediterranean seawater and an inflowing lower salinity North Atlantic Ocean water. Time-mean outflow and inflow estimated from direct current-meter observations have a volume flux of 0.97 and 1.01 Sv ($1 \text{ Sv} \equiv 10^6 \text{ m}^3 \text{ s}^{-1}$), respectively (Candela 2001).

The transport through the Strait of Gibraltar varies on a wide range of frequencies. Tidal currents are the most dominant and significantly modify the net flow through the strait. For instance, tides account for nearly one-half of the net Atlantic Ocean–Mediterranean Sea exchange because of correlation between tidal currents and the depth of the interface between the inflowing Atlantic and outflowing Mediterranean water masses (Bryden et al. 1994). The magnitudes of the inflow and outflow are also dictated by hydraulic control at the strait (Farmer and Armi 1986) and can vary between maximal and submaximal states of exchange (Garrett et al. 1990a; Send and Baschek 2001).

Fluxes associated with atmospheric pressure fluctuations dominate subinertial variations through the strait (Candela et al. 1989). To first order, the sea level of the Mediterranean Sea fluctuates according to an inverse barometer (Larnicol et al. 1995); sea level drops (rises) 1 cm when the atmospheric pressure rises (drops) by 1

Corresponding author address: Ichiro Fukumori, Jet Propulsion Laboratory, California Institute of Technology, M/S 300-323, 4800 Oak Grove Dr., Pasadena, CA 91109.
E-mail: fukumori@jpl.nasa.gov

mbar. Changes in the basin's water volume are balanced by changes in the net transport through the Strait of Gibraltar. Yet important deviations from an inverse barometer response have been observed, especially for periods shorter than a few days, possibly because of restrictions of flow through the straits (Garrett and Majaess 1984). In fact, Le Traon and Gauzelin (1997) demonstrate a measurable improvement in explaining observed sea level fluctuations of the Mediterranean Sea using the simple model of Candela (1991) that describes deviations from an inverse barometer due to friction at the Straits of Gibraltar and Sicily.

However, significant temporal sea level variations are often found even after accounting for fluctuating atmospheric pressure. These have been attributed to an inadequately modeled dynamic response of the Mediterranean Sea to atmospheric pressure fluctuations (Cazenave et al. 2002) or possibly to fluctuations driven by differences in evaporation and precipitation and internal hydraulic control at the Gibraltar Strait (Larnicol et al. 1995). For instance, Garrett et al. (1990a,b) and Ross et al. (2000) have postulated that observed sea level variability in and around the strait reflects flipping between maximal and submaximal states of the baroclinic exchange (Farmer and Armi 1986; Bormans et al. 1986). These hydraulic states are characterized by differences in the interface depth of the inflowing Atlantic water and outflowing Mediterranean water and by the consequent changes in sea level (Bormans and Garrett 1989). However, other observations, such as coincident hydrographic and sea level measurements in the western Mediterranean Sea, are inconsistent with the phase of such hypothesized switching (Garrett et al. 1990a,b).

In addition to atmospheric pressure-driven fluctuations, Garrett et al. (1989) identify a wind-driven component of the transport and sea level variability. In fact, although generally smaller than the pressure-driven fluctuations, on occasion the wind-driven transport can dominate the flow through the strait (García Lafuente et al. 2002b). However, the impact of this transport to sea level of the Mediterranean Sea as a whole is not entirely clear.

The present study investigates the basin-scale sea level variability of the Mediterranean Sea found as a residual to atmospheric pressure fluctuations. In particular, a new dominant mode of sea level oscillation is identified that is nearly uniform in phase and amplitude across the entire basin. Satellite altimeter observations and a numerical ocean general circulation model are utilized to study the nature and underlying mechanism of the variability that help reconcile existing observations.

In sections 2 and 3, we briefly describe the data and

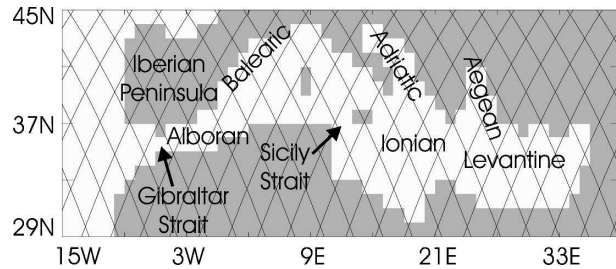


FIG. 1. Model domain and ground tracks of T/P in the Mediterranean Sea with the names of principal basins and straits. The white (gray) area is the modeled ocean (land) based on the model's grid for sea level. The entire model domain is global, as with T/P measurements.

the numerical model employed in this study, respectively. Observed and modeled sea level fluctuations are analyzed in section 4. The basin-wide sea level oscillation is first identified in section 4a. The effects of buoyancy forcing and winds are analyzed in sections 4b and 4c. In section 4d, a simple analytical model is put forth that describes the basin-wide fluctuation. The relationship between wind- and pressure-driven variability is examined in section 4e. A summary and conclusions are presented in section 5.

2. Sea level observations

Sea level observations of the Ocean Topography Experiment (TOPEX)/Poseidon (T/P) from 1993 to 2001 are used in this study. Figure 1 shows ground tracks of T/P in the Mediterranean Sea. Standard corrections are applied to the along-track satellite altimeter measurements including tides and inverse barometer corrections (Ponte et al. 1991). To facilitate the analysis, temporal anomalies of the along-track measurements are mapped to a uniform 1° grid in both latitude and longitude at 3-day intervals using a Gaussian weighting function (Fu 2004). The grids are located at 66.5°S – 66.5°N latitude and 0.5° – 359.5°E longitude. The Gaussian weight falls to one-half the maximum value at 1° , 2° , and 5 days in latitude, longitude, and time, using a search window of 3° , 12° , and 20 days, respectively. These mapped estimates are used throughout this study and are referred to as the altimetric measurements below. Possible deviations of the Mediterranean Sea from an inverse barometer response will be revisited in section 4e.

3. Model configuration

The model used in this study is based on the parallel version of the Massachusetts Institute of Technology

(MIT) ocean general circulation model (MITgcm; Marshall et al. 1997). The finite-difference primitive equation model employs advanced mixing schemes including *K*-profile parameterization (KPP) vertical mixing (Large et al. 1994) and Gent–McWilliams (GM) isoneutral mixing (Gent and McWilliams 1990).

The model employs an Arakawa C grid (Arakawa and Lamb 1977) and its domain is nearly global (73°S–73°N) with a uniform zonal grid spacing of 1° longitude. The meridional grid spacing is 0.3° latitude in the Tropics (within 10° of the equator) that gradually increases to 1° in the extratropics (poleward of 22° latitude). The total horizontal grid dimension is 360 zonally and 224 meridionally. There are 46 vertical levels with 10-m spacing within 150 m of the surface, gradually increasing to 400-m spacing at depth. The model bathymetry is based on the Earth Topography Five-Minute Grid (ETOPO5; NGDC 1988) by bin averaging the 5′ latitude and longitude ocean bathymetries to within the model resolution closest to one of the 46 levels. Figure 1 describes the model geometry of the Mediterranean Sea. As a finite-difference model, the present model represents processes averaged over its grid resolution and does not accurately simulate variabilities smaller than the size of its grid (e.g., local sea level variability within the Strait of Gibraltar). However, the model can be expected to reasonably simulate aspects of large-scale averages and their variability. In fact, as discussed in the following sections, despite its limited spatial resolution, the model is fairly capable at simulating the basin-wide fluctuation of the Mediterranean Sea.

The model employs a free-slip boundary condition, an implicit free surface, and is forced by 12-hourly surface wind stress and daily heat and freshwater fluxes. The fluxes are based on the reanalysis products of the National Centers for Environmental Prediction–National Center for Atmospheric Research (NCEP–NCAR; Kalnay et al. 1996) (approximately 2° spatial resolution), except that the time means, computed between 1993 and 1996, are replaced by the corresponding climatological products of the Comprehensive Ocean–Atmosphere Data Set (COADS; da Silva et al. 1994). Additionally, model sea surface temperature (SST) and sea surface salinity (SSS) are relaxed toward the NCEP–NCAR SST analysis and the climatological mean SSS of Boyer and Levitus (1998), respectively. SSS is relaxed with a time scale of 60 days, whereas SST is relaxed to observed values using a spatially varying time scale, typically between 1 and 2 months, based on the method of Barnier et al. (1995). Freshwater fluxes (evaporation, precipitation, river runoff) are implemented as a virtual salt flux in which the surface salinity

is modified in accordance with the freshwater forcing as opposed to changing the model’s freshwater volume.

The model is integrated (1-h time step) using the forcings from 1980 to the present, following a 10-yr spinup. The spinup was run from rest with a climatological temperature and salinity distribution (Boyer and Levitus 1998) and was forced by the seasonal climatological forcings (COADS). Model results are saved as 10-day averages at 10-day intervals. In addition, the sea level and bottom pressure are saved at 12-h intervals to better resolve the high-frequency barotropic fluctuations (e.g., Fukumori et al. 1998).

This model has been configured for data assimilation as part of the Consortium for Estimating the Circulation and Climate of the Ocean (ECCO; Stammer et al. 2002). Model-estimated fields of both the simulation and assimilation are available online (http://www.ecco-group.org/data_server.html). Here we employ the results of the model simulation described above to analyze the observed variations of the Mediterranean Sea independent of the oceanic measurements. Other examples of these model results, both for the simulation and assimilation, can be found in Lee et al. (2002), Dickey et al. (2002), Lee and Fukumori (2003), Gross et al. (2003, 2004), Fukumori et al. (2004), Wang et al. (2004a,b), and Kim et al. (2004).

4. Sea level variability of the Mediterranean Sea

The large-scale sea level variability of the Mediterranean Sea is dominated by a nearly uniform change across the basin. In particular, some of these changes occur over a relatively short period of time. Figure 2 shows an example of the sea level change of the Mediterranean Sea and portions of the North Atlantic Ocean based on the altimetric measurements (section 2). While the sea level of the North Atlantic Ocean in Fig. 2 changes gradually in time, that of the Mediterranean Sea decreases by as much as 15 cm in less than 12 days. Such rapid changes of the Mediterranean Sea often appear as sudden flickering of the entire basin in time series animations of sea level. The nature of these fast fluctuations and other large-scale sea level variations are examined in the following sections using the altimetric measurements and the numerical ocean circulation model (section 3).

a. Basin-wide sea level oscillation

To characterize the spatial scale of the variability, empirical orthogonal functions (EOFs) are computed for both altimetric measurements and model sea level variability. Figure 3a shows the first EOF of the altimetric sea level of the Mediterranean Sea. Sea levels in

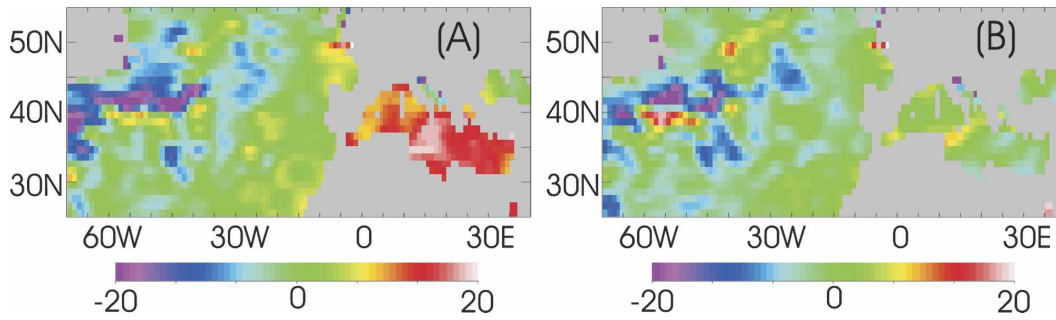


FIG. 2. An example of rapid sea level change of the Mediterranean Sea. Shown are sea level anomalies from the 8-yr mean (1993–2001) based on altimetric measurements (cm) for (a) 7 and (b) 19 Jan 1996.

the Atlantic Ocean, the Black Sea, the Adriatic Sea, and the Aegean Sea are excluded from this EOF analysis as the variabilities in these regions are largely uncorrelated with the rest of the Mediterranean Sea (see Fig. 2 and also Fig. 5a below). Illustrating the dominant basin-wide fluctuation, the first mode is nearly uniform

in amplitude across the basin and accounts for 75% of the basin-wide variance. The second mode (not shown) accounts for 14% and describes differences between the Levantine and Ionian Basins. (See Fig. 1 for the principal basins and straits of the Mediterranean Sea.)

The temporal variability of the first EOF (first prin-

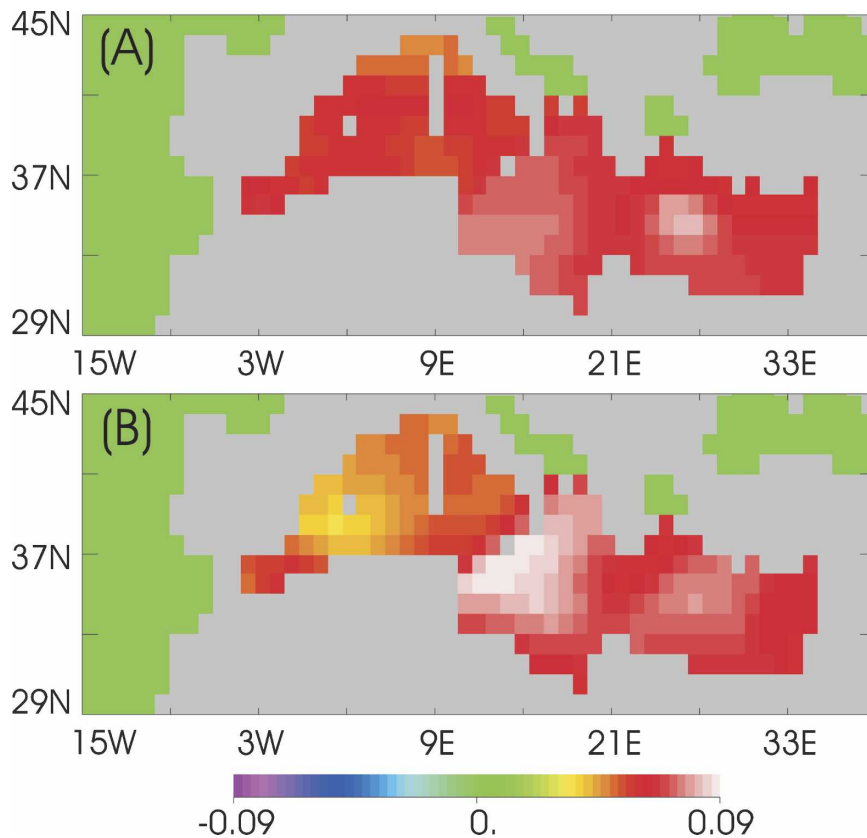


FIG. 3. EOFs of T/P sea level variability across the Mediterranean Sea: (a) total and (b) nonseasonal variability. Sea levels in the Atlantic Ocean, Black Sea, Adriatic Sea, and Aegean Sea are excluded from this EOF analysis. The modes are normalized to unit norm over the Mediterranean Sea as defined by the mapped observations.

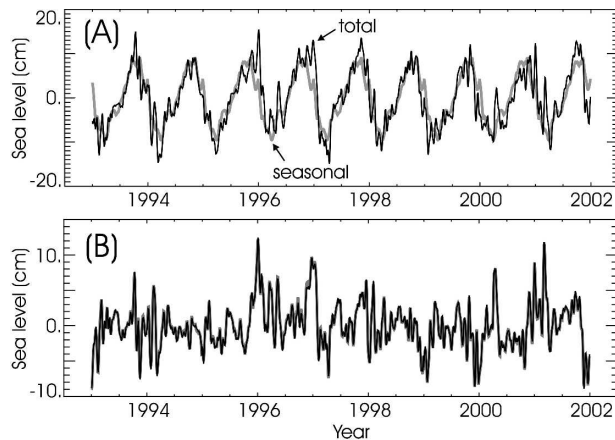


FIG. 4. Time series of T/P basin-mean sea level variability: (a) total variability (black) and its average seasonal cycle (gray) and (b) anomaly from average seasonal cycle (black) and the first principal component of nonseasonal variability (gray). The two curves in (b) are practically indistinguishable from each other. (The principal component is scaled to have the same variance as the nonseasonal mean sea level variability.) The standard deviation of the time series is 6.5 cm (black) and 5.6 cm (gray) in (a) and 3.2 cm in (b).

principal component) describes changes in the basin-mean sea level of the Mediterranean Sea; in fact, the two are practically identical to each other (correlation coefficient is 1.00). Time series of the basin-mean sea level has a standard deviation of 6.5 cm and is dominated by the seasonal cycle (Fig. 4a); the mean sea level is highest in autumn (November) and lowest in spring (April). Apart from this seasonal cycle, the time series also shows relatively short time-scale intraannual variability of order 20 days and longer. Some of these amplitudes are larger than 10 cm and are comparable to the magnitude of the seasonal cycle itself.

Figure 4b shows time series of this nonseasonal basin-averaged sea level obtained as an anomaly relative to the average annual cycle computed over the 9-yr data period. Empirical orthogonal functions of these nonseasonal oscillations have similar structures to those for the total sea level. The first EOF (Fig. 3b) accounts for 54% of the nonseasonal variance and has a slightly larger amplitude variation within the basin than that of the total variability (Fig. 3a). Nevertheless, its principal component is indistinguishable from the corresponding basin-averaged sea level (Fig. 4b; correlation is 1.00). The standard deviation of this nonseasonal basin-mean sea level variability is 3.2 cm, whereas that of the average seasonal cycle is 5.6 cm.

The nonseasonal basin-wide sea level fluctuation is largely confined to within the Mediterranean Sea. Figure 5a shows the correlation between the nonseasonal basin-mean sea level and sea level anomalies at differ-

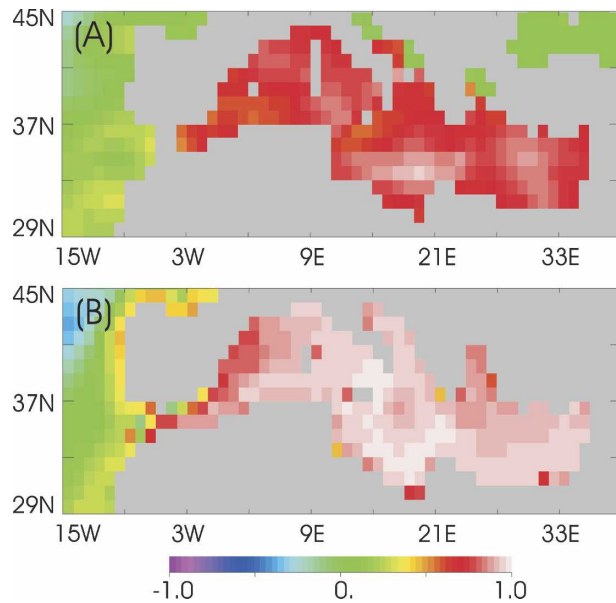


FIG. 5. Correlation coefficient between nonseasonal anomalies of sea level and their basin average of the Mediterranean Sea: (a) T/P measurements and (b) model simulation.

ent locations. The correlation is high and nearly uniform within the Mediterranean Sea and reflects the dominant mode of the basin's variability. In comparison, the sea levels in the Atlantic Ocean and the Black Sea, as well as that in the Adriatic and Aegean Seas, are practically uncorrelated to this mode. [The total basin-mean fluctuation is correlated to sea level outside the basin (not shown) because of similar annual fluctuations due to seasonal heating and cooling.]

Despite its coarse resolution, the model is fairly skillful in simulating the observed variability. Figure 6a shows the model's first EOF that is equivalent to that of the altimetric observation given in Fig. 3. (The model EOFs are computed over the entire Mediterranean Sea including the Adriatic and Aegean Seas.) This first mode accounts for 85% of the variance and, as in the observations, describes a nearly uniform variation across the basin. The second mode (not shown) accounts for 6% of the variance and describes differences between the Levantine and Balearic Basins.

Similar to altimetric measurements, the first EOF of the model's nonseasonal variability (Fig. 6b) also describes a basin-wide fluctuation that is nearly the same as that of the total sea level (Fig. 6a). This first EOF accounts for 82% of the nonseasonal variance. Moreover, the first principal components of both total and nonseasonal fluctuations (not shown) are indistinguishable (correlation coefficient is 1.00) from the model's corresponding basin-averaged sea level variability (Fig. 7).

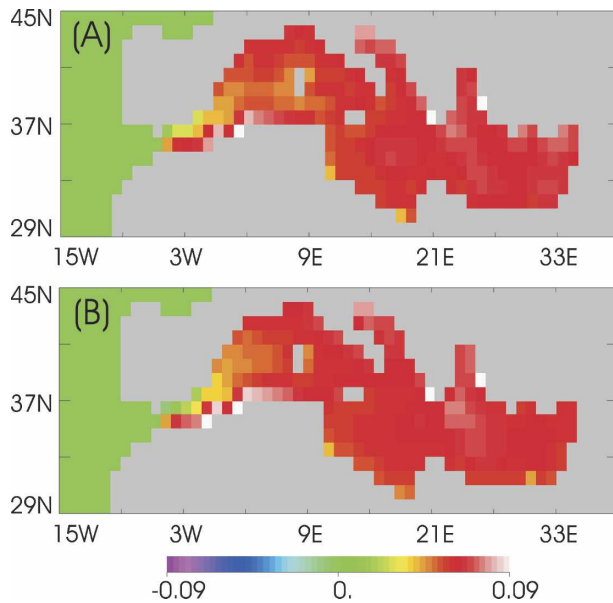


FIG. 6. First EOFs of model sea level variability across the Mediterranean Sea: (a) total and (b) nonseasonal variability. The EOFs are computed for sea level within the basin east of and not including 5.5°W (the narrowest grid point of the model's representation of the Gibraltar Strait), and are normalized to unit norm over this region defined by the model grid.

Although comparable to first approximation, the structure of the model's basin-wide mode of oscillation (Fig. 6b) is slightly more uniform than that of the observations (Fig. 3b). For instance, observations have larger EOF amplitude variations in the Balearic and Ionian Basins. The relative spatial homogeneity and the larger variance that the model's EOF explains in comparison with that of the satellite data may be due to the model's deficiency in simulating variability as a result of its limited spatial resolution. Alternatively, the observations' relative spatial inhomogeneity may also be due to aliasing of high-frequency oscillations; TOPEX/Poseidon has a 10-day repeat cycle in sampling the Mediterranean Sea illustrated in Fig. 1.

Similar to the observations, the model's nonseasonal basin-wide variability is mostly confined to within the Mediterranean Sea as evidenced by the correlation shown in Fig. 5b. The correlation between the model sea level and its basin mean (Fig. 5b) being higher than that in the observations (Fig. 5a) reflects the larger fraction of variance that the basin mode explains for the former as compared with the latter. The model correlation also extends farther into the Adriatic and Aegean Seas than does that in the observations, which may be due to a lack of model resolution. For instance, seiches are a significant component of sea level variability in the Adriatic Sea (e.g., Leder and Orlić 2004) and the

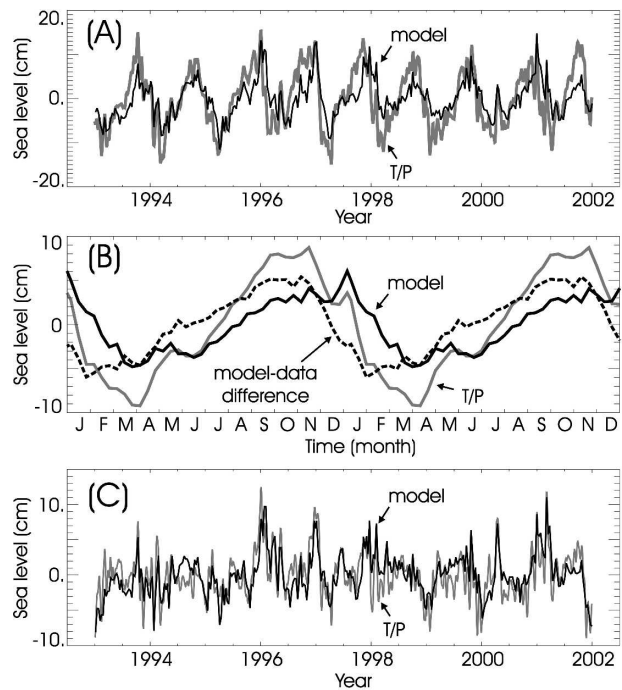


FIG. 7. Time series of basin-mean model (black) and observed (T/P; gray) sea level: (a) total variability, (b) mean seasonal cycle, and (c) anomaly from the mean seasonal cycle. Dashed curve in (b) is the difference between the mean seasonal cycles of the altimeter measurements and of the model. Observed variabilities in gray are the same as those shown in Fig. 4 as black curves. The model's standard deviations are 4.3 (a), 3.1 (b), and 3.1 cm (c). Correlation coefficients between the model and the altimetric observations are 0.75 (a), 0.81 (b), and 0.75 (c).

Aegean Sea is dominated by numerous small islands. However, the present model lacks the spatial resolution necessary to resolve these scales and processes. The model correlation is also higher than the observation's along the shallow coastal regions around the Iberian Peninsula in the Atlantic Ocean. This difference along the coast may also be due to inaccuracies of the model and/or errors in the altimetric measurements near coastal boundaries (e.g., mapping errors).

As in the observations, the model's basin-mean sea level is dominated by the seasonal cycle, but it has a slightly smaller total standard deviation (4.3 cm) than the altimetric measurements (6.5 cm) (Fig. 7a). This discrepancy is principally due to differences in the average seasonal cycle; the model's seasonal cycle (Fig. 7b) has a standard deviation of 3.1 cm in comparison with the observation's 5.6 cm. Moreover, the average seasonal cycle has an apparent phase difference between the two. Although the minimum is achieved at similar instances [yearday 95 (April) for altimeter measurements based on 10-day averages, and yearday 85 (March) for the model], the maximum for the altimeter

measurements occurs in November (yearday 315) whereas the model reaches its maximum in December (yearday 365). The difference between the two (altimeter minus model; dashed curve in Fig. 7b) has a standard deviation of 3.6 cm with a maximum and minimum in November (yearday 305) and January (yearday 25), respectively. The nature of this difference is not entirely clear, but suggests possible inadequacies of the model. For instance, the model lacks the spatial resolution to accurately simulate the hydraulic control mechanism thought to regulate baroclinic exchange through the Strait of Gibraltar (e.g., Bormans et al. 1986). As is common with models using the Boussinesq approximation, the model also treats external freshwater fluxes as a forcing on the model salinity (i.e., virtual salt flux) as opposed to changes in the model's net freshwater volume (cf. section 2). Such model limitations may contribute to the model's incomplete simulation of the seasonal variability.

In contrast to the mean seasonal cycle, the model's nonseasonal variability is comparable to that of the altimetric data (Fig. 7c), with standard deviations of 3.1 and 3.2 cm, respectively. Correlation coefficients between the basin-mean sea levels of the model and altimetric data are 0.75 for both the total (Fig. 7a) and nonseasonal variabilities (Fig. 7c) and 0.81 for the mean seasonal cycle (Fig. 7b). In terms of variance, the model explains 55% and 51% of the observed total and nonseasonal variabilities, respectively.

Figure 8 shows the spectra and coherence of the basin-averaged sea level variability. For clarity, the spectra are shown for nonseasonal fluctuations in variance-preserving form, while the coherence amplitude and phase include the seasonal cycle. (Otherwise, the seasonal cycle dominates the spectra.) Note that the average seasonal cycles removed from the spectra are not strictly harmonic (Fig. 7).

The model has slightly less energy than the observations at periods between 160 days (0.006 cpd) and 30 days (0.03 cpd) but has comparatively more variance at periods shorter than 25 days (0.04 cpd). Such differences may be due in part to the satellite's 10-day sampling (20-day Nyquist period) and the possible aliasing of higher-frequency variability. In fact, the model is significantly coherent with the observations, except for time scales shorter than the Nyquist period (20 days, 0.05 cpd) where the coherence is marginally significant at the 95% confidence level (Fig. 8b). Interestingly, the model has an elevated coherence near 16 days (0.06 cpd), the reason for which is not entirely clear. The phase of the model is nearly coincident with the observations except at periods longer than 110 days (0.009

cpd) where the observations lead the model by approximately 40°.

Given the similarity between the model and the observations, especially the nonseasonal variability, the model provides a means to explore the nature of the observed nearly uniform sea level fluctuation of the Mediterranean Sea and will be analyzed in the following sections. The inverse barometer correction also shown in Fig. 8 will be discussed later in section 4e.

b. Buoyancy-driven changes versus wind-driven changes

To discern the relative effects of buoyancy forcing and wind, the same model simulation is repeated but forced with time-mean winds instead of time-varying winds, thus isolating the effects of variable buoyancy forcing. The difference between the original model integration and this buoyancy-driven simulation (i.e., the residuals) represents the effects of time-variable wind forcing.

The resulting buoyancy-driven basin-mean sea level change (green curves in Fig. 9) is dominated by a slowly varying seasonal cycle with small nonseasonal fluctuations. In comparison, the residual wind-driven component is more irregular with significant interannual and intraannual variability (red curves in Fig. 9). In fact, wind forcing accounts for practically all nonseasonal basin-mean sea level fluctuations (Fig. 9c).

The buoyancy-driven fluctuation is a major component of the seasonal cycle, but it is slightly out of phase with the total variability (black curve in Fig. 9b). Although both buoyancy-driven and total sea level changes have their minimum in March, the maxima are reached in September and December, respectively. This difference is due to the seasonal wind-driven fluctuation (2.7-cm standard deviation) that has an amplitude similar to the buoyancy-driven component (2.9 cm). This residual wind-driven change has a minimum in July and a maximum in December.

The wind-driven basin-wide sea level variability is largely associated with barotropic changes of the Mediterranean Sea. For instance, basin-averaged bottom pressure anomalies (cyan curves in Fig. 9), in terms of equivalent sea level changes, are nearly coincident with the residual sea level variability (red curves in Fig. 9). This correspondence between bottom pressure and sea level indicates that the residual sea level fluctuation is a wind-driven depth-independent barotropic change of the entire basin. This in turn implies changes in the net inflow and outflow of the water volume through the Strait of Gibraltar. In fact, the model's time-integrated net volume transport through the strait is comparable to the model-simulated volume change of the Mediter-

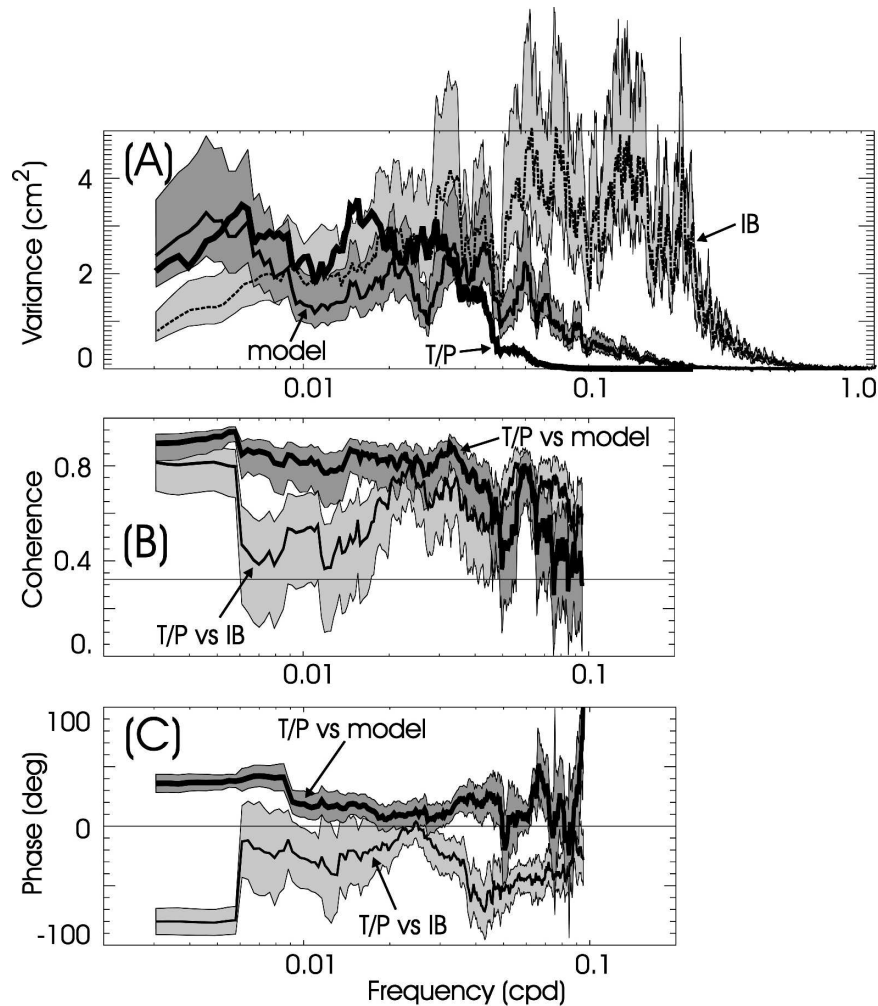


FIG. 8. (a) Variance-preserving spectra of basin-mean sea level of T/P measurements (thick black), model simulation (thin black), and inverse barometer correction (IB) (thin dotted). (b) Coherence amplitude and (c) phase between the altimetric observations and model (thick) and the former and IB correction (thin). For clarity, the spectra in (a) are for nonseasonal fluctuations while the coherence and phase include the seasonal cycle. The gray areas denote the 90% confidence intervals (Koopmans 1974, chapter 8). (Confidence intervals for T/P spectra are omitted for clarity.) Positive (negative) phase in (c) indicates altimetric observations leading (lagging) the time series. Line at 0.32 in (b) is the 95% confidence limit of the zero coherence; anything above the line is statistically significant at the 95% limit. All estimates are based on averaging 21 neighboring frequencies. See section 4e for a discussion of the IB correction.

ranean Sea (Fig. 10a). Differences between the sea level change and volume “flux” in Fig. 10a can be ascribed to buoyancy-driven processes, including air–sea fluxes, and to temporal changes of temperature and salinity within the strait.

The corresponding velocity within the strait is not terribly large and is plausible (Fig. 10b). The 10-day-mean depth-averaged zonal velocity (volume transport) in the modeled strait has a standard deviation of 2.9 mm s^{-1} (0.10 Sv) and is dominated by higher-frequency

variability than the basin-averaged sea level change. The maximum sea level change simulated by the model over 10 days is 8.6 cm and occurs in February 2001. The corresponding 10-day-mean depth-averaged velocity (volume transport) in the strait is 7.6 mm s^{-1} (0.26 Sv), using the model’s area of the Mediterranean Sea and the depth and width of the strait of $2.6 \times 10^6 \text{ km}^2$, 303 m, and 111 km, respectively. For the actual strait, this maximum volume change would imply an 8.1 cm s^{-1} depth-averaged current near the sill where the cross-

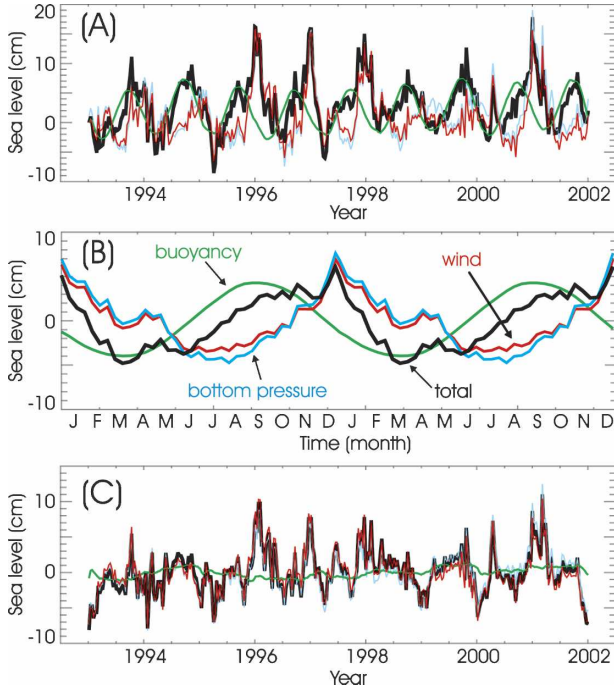


FIG. 9. Time series of (a) model basin-mean sea level, (b) its mean annual cycle, and (c) anomalies from the mean annual cycle: reference model (total; black), buoyancy-driven model (green), and residual (reference minus buoyancy-driven model representing wind-driven variability; red). Basin-mean ocean bottom pressure of the reference model is also shown as the cyan curve in equivalent sea level. Units: cm. The four curves are shown in all panels. In (c), all except the green buoyancy-driven estimate nearly coincide with each other. See (b) for legend.

strait area is minimum ($3.16 \times 10^6 \text{ m}^2$; Bryden et al. 1994). These fluctuations are realistic and are much smaller than other fluctuations observed by current measurements within the strait (e.g., García Lafuente et al. 2002a). See section 4e for additional discussion about fluxes through the Strait of Gibraltar.

c. What wind drives the basin-wide sea level variability?

The winds responsible for the wind-driven basin-wide sea level oscillation can be conveniently analyzed by the adjoint of the model. The model adjoint provides an efficient means of evaluating the sensitivity of a model quantity to various model variables (controls). For instance, using the adjoint of the MITgcm in a configuration different from the present study, Marotzke et al. (1999) evaluated the sensitivity of the heat transport across the Atlantic Ocean to prior model states at various instances. Fukumori et al. (2004) used the adjoint of a passive tracer to analyze the origin and pathway of water occupying the surface layer of the eastern equatorial Pacific Ocean.

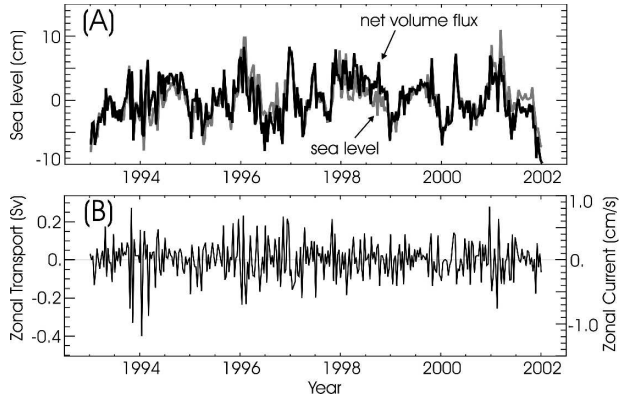


FIG. 10. Model time series of (a) nonseasonal net time-integrated zonal volume flux through the Strait of Gibraltar (35.5°N , 6°W in the model; black curve) and (b) the depth-averaged velocity (and volume flux) through the strait. Net volume flux in (a) is shown in terms of the implied mean sea level change of the Mediterranean Sea. The gray curve in (a) is the actual nonseasonal component of the model basin-mean sea level (same as black curves in Figs. 7c and 9c).

Junge and Haine (2001), using an adjoint of another model, evaluated the sensitivity of the sea surface temperature of the North Atlantic Ocean to prior ocean states and to prior air–sea forcings.

Here, we evaluate the dependency of the Mediterranean Sea basin-averaged sea level to winds at various locations and at various times using the adjoint of the present model (section 3). In particular, we examine the linearized sensitivity of 10-day-averaged basin-mean sea level to winds at various locations and prior instances up to a 1-yr lag (including coincident winds) but, for simplicity, time invariant over 10-day intervals. Mathematically, this sensitivity can be written as

$$\frac{\partial}{\partial f_{10d}(x, y, T - N)} \int \bar{h}(T) dS/S_{\text{Med}}, \quad (1)$$

where $h(T)$ is the model sea level at time T and $f(x, y, T - N)$ is either the zonal or meridional wind at the horizontal location (x, y) at time N prior to time T . The overbar denotes a 10-day average and the subscript $10d$ denotes a time-invariant variable over a 10-day interval. The integration is carried out over the area S of the Mediterranean Sea, where S_{Med} is its total horizontal area. Assuming stationarity, Eq. (1) is independent of time T . See the appendix for mathematical details of such calculation.

Figure 11 describes the geographic variation of such sensitivity [Eq. (1)] at lags of 0 and 20 days. Locations with nonzero values identify places where winds cause changes in the basin-mean sea level. The largest sensi-

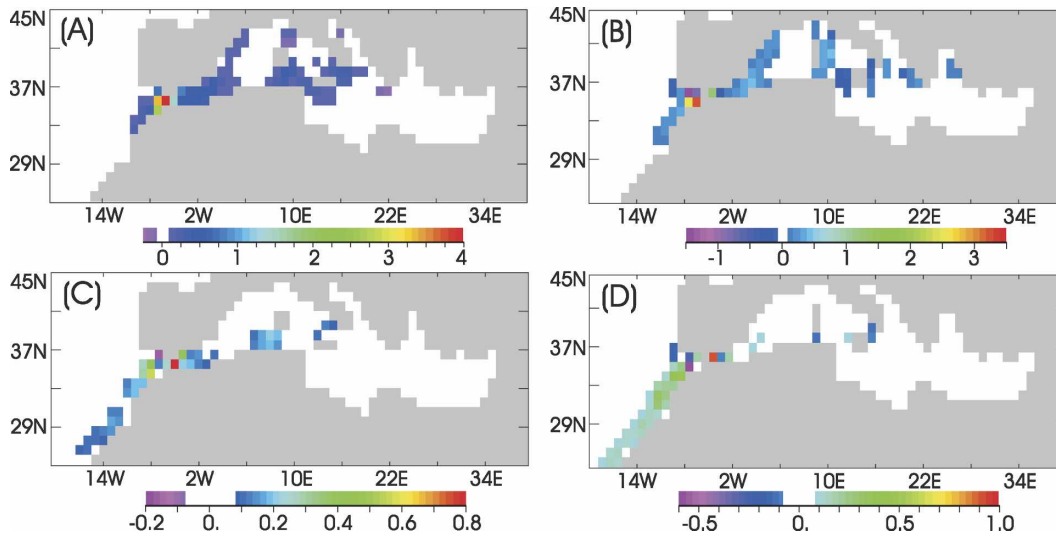


FIG. 11. Sensitivity [Eq. (1)] of basin mean sea level to (a), (c) zonal and (b), (d) meridional wind stresses. Values at each location indicate changes in the mean sea level over the entire Mediterranean Sea due to unit wind stress perturbations at that model grid location at particular time lags. The panels do not show a geographical variation of sea level but rather a geographical variation of this sensitivity. Sea level and wind represent a 10-day average and a 10-day time-invariant quantity, respectively. Panels (a) and (b) are coincident 10 days [$N = 0$ days in Eq. (1)] whereas panels (c) and (d) are the sensitivity of the sea level to winds 20 days prior ($N = 20$ days). Units are in centimeter meters squared per newton and describe the change in sea level in centimeters per unit wind stress change in newtons per meter squared. Note the different scales used among the panels. Magnitudes smaller than $0.08 \text{ (cm m}^2\text{)} \text{ N}^{-1}$ are omitted for clarity in all panels. See text for further details.

tivity is found with respect to the zonal wind stress within the Strait of Gibraltar at 0-day lag (Fig. 11a), that is, coincident winds. In particular, a 1 N m^{-2} eastward wind stress anomaly over a 10-day interval within a $1^\circ \times 1^\circ$ square (model resolution) in the strait at 35.5°N , 6°W results in a 4-cm increase in the basin-mean sea level averaged over the same 10-day period. That this sensitivity (not local sea level) is nearly zero over most of the Mediterranean Sea and the Atlantic Ocean well away from the strait indicates that the basin-mean sea level is insensitive to winds at those locations.

At 0-day lag, the sensitivity to zonal wind stress is positive throughout the strait and its neighboring regions (Fig. 11a); that is, eastward wind stress results in an increase in the Mediterranean sea level. In comparison, for meridional winds, the mean sea level is most sensitive to its convergence immediately outside (west of) the strait (Fig. 11b).

The sensitivity to winds 20 days prior (Figs. 11c and 11d) is smaller in magnitude than those at 0-day lag, but extends farther southward along the African coast, but not north of the strait. This can be understood as being due to wind-driven coastal Kelvin waves and their anisotropic propagation. Only coastal Kelvin waves generated to the south can propagate to the strait and affect its net transport at a later instant (20 days for

Figs. 11c and 11d). That the sensitivity at larger lags (Figs. 11c and 11d) is much smaller than at zero lag (Figs. 11a and 11b) indicates that the adjustment time scale for the wind-driven basin-wide sea level change is shorter than 20 days (time interval in the figure) and that the basin-mean sea level is in near-stationary balance with the wind.

The accuracy and consistency of these sensitivity measures are demonstrated in Fig. 12 by comparing the model-simulated sea level with that evaluated by a convolution of 10-day-averaged wind stress anomalies and the computed adjoint sensitivities [Eq. (1)]. (See the appendix for details.) Differences between the two are small and can be ascribed to fluctuations shorter than 10 days and to model nonlinearities. The nonlinearities include those of the model physics (e.g., total sea level variability is not identical to the sum of the wind- and buoyancy-driven simulations evaluated separately) and of the linearization underlying the adjoint model.

Winds in the Strait of Gibraltar and its neighboring region account for most of the simulated variability. Figure 13 shows the percentage of the Mediterranean Sea mean sea level variance accounted for by winds at each location (model resolution of 1° square). The largest single point contribution is found within the strait and at its western mouth at 35.5°N , 6°W and 35°N , 5.5°W for zonal and meridional winds, respectively.

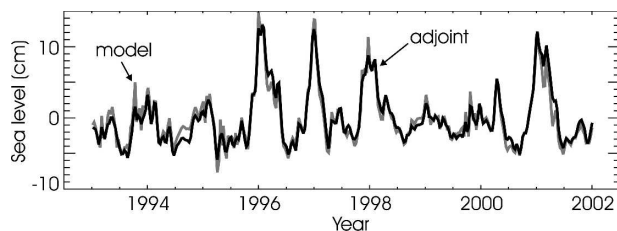


FIG. 12. Time series comparison of wind-driven basin-mean sea level variability based on the adjoint sensitivity (black) and that simulated by the model (gray).

Winds within 1° (model resolution) of these locations each account for 16% of the total basin-mean sea level variance. Although winds within the strait and its immediate vicinity have the largest effect per unit area, winds near but away from the strait collectively account for as large a fraction of the basin-wide sea level variability as that at the strait. This outside region includes the Alboran Sea and the Atlantic Ocean immediately to the west of the strait between the Iberian Peninsula and Africa, where winds contribute approximately 2%–6% of the total basin-mean sea level variance per 1° square. The total contributions from the zonal and meridional winds in the vicinity of the strait defined by a 12° zonal by 5° meridional area indicated in the inset in Fig. 13 account for more than 74% and 36% of the total variances, respectively. (The skills do not add to 100%

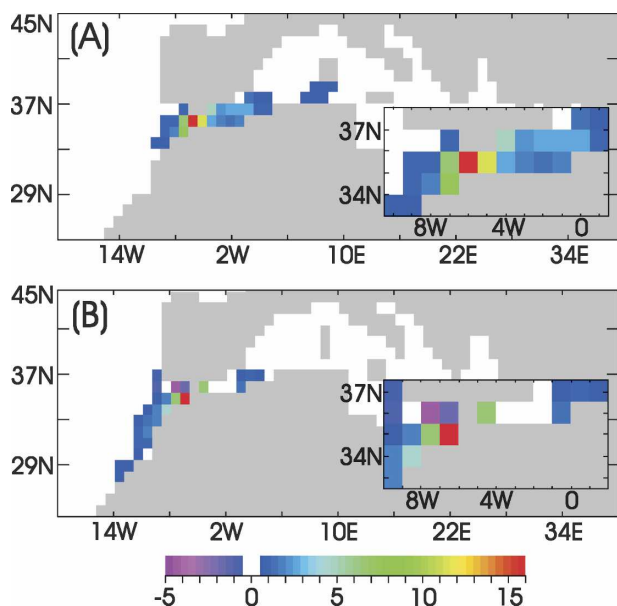


FIG. 13. Percentage of variance of the simulated wind-driven basin-mean sea level variability accounted for by wind at different model grid locations: (a) zonal and (b) meridional wind. Inset shows details in the vicinity of the Gibraltar Strait. Magnitudes smaller than 0.5% are omitted for clarity. Values in the eastern Mediterranean are uniformly smaller than 0.5%.

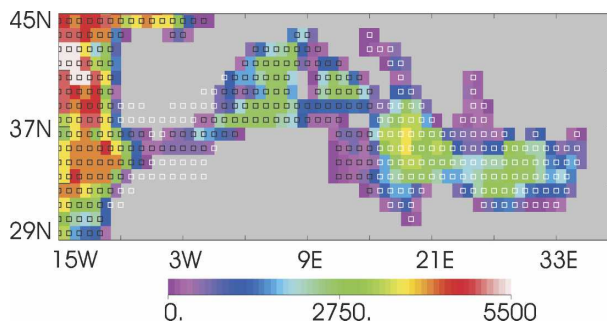


FIG. 14. Model grid over the Mediterranean Sea. The square symbols denote the zonal velocity grid. The color indicates the depth of the model ocean. The gray area is land. White symbols over land in the vicinity of the Strait of Gibraltar and those in the eastern Mediterranean Sea are treated as ocean and land points, respectively, in experiments described in section 4d.

because winds are spatially correlated.) The skill's frequency dependence is relatively small (not shown); that is, the relative skill of the winds for accounting for the simulated wind-driven annual variability and for simulating the rest of the fluctuation are nearly the same as the skill for the total variability illustrated in Fig. 13.

The large skill of the winds in the region surrounding the strait is largely due to the inhomogeneity in the ocean's dynamics as opposed to the particularly large wind fluctuations within the strait. The largest sensitivity as measured by the squared time integral of the adjoint sensitivity [Eq. (1)] from 0- to 1-yr lag is found in the vicinity of the strait similar to where most of the actual contributions arise (Fig. 13).

d. Model geometry and dynamics

The model's skill in simulating the observed Mediterranean Sea basin-mean sea level fluctuation (Fig. 7) is somewhat remarkable considering the present model's relatively coarse spatial resolution. In particular, the Strait of Gibraltar, which is approximately 13 km wide across its narrowest point, is represented in the model by a single grid point in the meridional direction that is 111 km wide (black symbols in Fig. 14). Part of the reason for the model's skill rests in the fact that the basin-wide fluctuation depends not only on winds within the strait but also on winds outside the strait (section 4c; Fig. 13). To gain further insight into the dynamics of the fluctuation, additional experiments are conducted to analyze the sensitivity of the model simulation to the particular geometry of the strait and that of the Mediterranean Basin.

In one experiment, the Strait of Gibraltar and its surrounding basins (the Alboran Sea and Atlantic Ocean immediately to the west of the strait) are widened north and south by two model grid points (2°

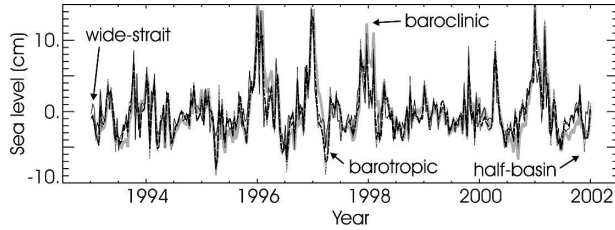


FIG. 15. Wind-driven variability (cm) of the basin-mean sea level for different configurations of the model: wind-driven baroclinic (gray), barotropic (dashed), wide strait (thin solid black), and half basin (dotted). All curves are based on 12-hourly model results and are nearly identical to each other.

latitude) in each direction (white symbols in Fig. 14 in the vicinity of the Gibraltar Strait). The depth of the widened region is set to the same value as the adjacent ocean points to the south and north, respectively, which is approximately 300–400 m. In another experiment, the area of the Mediterranean Basin is halved by treating regions east of Sicily as land (east of 16.5°E; white symbols in Fig. 14 in the eastern Mediterranean Sea). To eliminate the slow baroclinic adjustments and to isolate the barotropic variability that underlies the basin-wide oscillation (section 4b), both experiments are initialized at rest with a uniform temperature and salinity distribution (20°C, 35 psu) and are forced solely by winds. To isolate the impact of the basin geometry, as a reference, the same barotropic experiment is also conducted using the same model geometry as the baroclinic experiments discussed in previous sections.

In all three experiments, the sea level of the Mediterranean Sea is dominated by basin-wide fluctuations similar to the baroclinic experiment described in the preceding sections. In each of these barotropic experiments, and in others described below, the dominant empirical orthogonal function has a nearly uniform amplitude across the Mediterranean Basin (or its equivalent) and accounts for more than 95% of their respective basin-wide sea level variances. Their corresponding principal components are practically indistinguishable (except in amplitude as the principal components are nondimensional) from time series of their respective mean sea levels of the corresponding Mediterranean Basin.

As seen in Fig. 15, time series of the basin-mean sea level fluctuation of these barotropic experiments are fairly similar to that of the wind-driven component of the original baroclinic model. Comparisons among the experiments are summarized in Table 1. For instance, the standard deviation of the reference barotropic model is 3.6 cm and has a correlation coefficient of 0.93 with the wind-driven component of the original baroclinic model, which has a standard deviation of 4.1 cm.

TABLE 1. Correlation and standard deviation (σ) of the mean sea level variability of the barotropic experiments. The five experiments differ in their bottom topography and coastal geometry: 1) reference geometry (section 2), 2) wider Gibraltar Strait, 3) half-size Mediterranean basin, 4) half-depth Gibraltar Strait, and 5) uniformly deep Gibraltar Strait and Mediterranean Basin. Experiment 6 uses the same reference geometry but with no rotation (zero Coriolis force). Correlation is between each experiment and the reference barotropic calculation (expt 1), except for expt 1 itself, which lists the correlation with the wind-driven variability of the baroclinic experiment.

Expt	Correlation	σ (cm)
1) Reference configuration	0.93	3.6
2) Widened strait	0.84	3.2
3) Halved basin	0.97	3.9
4) Shallow strait	0.97	5.6
5) Deepened strait and basin	0.56	0.6
6) No rotation	0.76	2.2

The similarity between these two experiments reflects the dominant linear barotropic nature of the basin-wide fluctuation described in the preceding section.

As is evident by visual comparison (Fig. 15), the mean sea levels of the two experiments with modified geometry have significant correlation with and similar amplitudes to the reference barotropic model (Table 1). Apparently, the mean sea level fluctuation of the Mediterranean Sea is not particularly sensitive to the detailed geometry of the basin or to the width of Gibraltar Strait and its neighboring region.

These experiments and the sensitivity discussed in section 4c suggest a possible regional dynamic balance between the sea level difference of the two basins and the wind forcing across the region connecting the basins, which is independent of the details of the basin geometry. In particular, the strong dependence of the basin mean sea level on the coincident zonal wind stress suggests a stationary balance between stress (wind) and pressure gradient in the along-strait direction, such that

$$\frac{\partial \tau_x}{\partial z} \approx \frac{\partial p}{\partial x}, \quad (2)$$

where τ_x is the stress in the along-strait direction (x), p is the pressure, and z is the vertical coordinate. The forcing region, according to the analysis in section 4c, is the area connecting the Mediterranean Sea and the Atlantic Ocean and includes the Alboran Sea and the Atlantic Ocean immediately to the west of the strait, and not only the Strait of Gibraltar itself (Fig. 13a).

Dynamically speaking, the meridional scale of the connecting region is too small to support a large-scale geostrophic balance in the along-strait direction. Instead, an along-strait wind perturbation [stress at the

surface, $\tau_x(0)$] generates a downwind net transport through the strait until a pressure head develops between the two ends of the connecting region that balances the wind forcing [Eq. (2)]. The sea level (surface pressure) within each ocean basin responds uniformly to this net transport, via a fast barotropic adjustment conserving volume, similar to the effects of atmospheric pressure forcing (i.e., inverse barometer effect) and of surface freshwater fluxes (e.g., evaporation, precipitation, river runoff). The sea level changes outside the Mediterranean Sea in response to such a net exchange is small because of the much larger surface area of the global ocean in comparison with that of the Mediterranean Sea.

Integrating Eq. (2) horizontally and vertically within the strait and the neighboring region that connects the Mediterranean and Atlantic basins gives

$$WL\tau_x(0) \approx \rho gWD\Delta h, \quad (3)$$

or, alternatively,

$$\Delta h \approx \frac{L}{\rho gD} \tau_x(0), \quad (4)$$

where we have assumed a hydrostatic balance and, for simplicity, a uniform wind and a rectangular region (width W , length L) with constant depth D . Here, ρ and g are water density and gravity, respectively, and Δh is the sea level difference between the two ends of the connecting region, or equivalently that of the two basins connected by the strait and its neighboring seas (positive when increasing in the x direction).

Consistent with the experiments above, Eq. (4) shows that the sea level difference between the two basins is independent of the connecting region's (strait's) width W and of the size of each basin. In comparison, the difference is proportional to the length of the connecting region; the larger the area in the direction of the wind, the larger the effective forcing and the larger the sea level difference.

However, somewhat counterintuitively, Eq. (4) also suggests that the sea level difference is inversely proportional to the depth of the connecting region; a shallower strait causes a larger net wind-driven transport resulting in a larger sea level difference. To test this analysis, an additional barotropic simulation is performed reducing the bottom depth within the strait and its surrounding region (8.5° – 2.5° W) to half the value of the reference configuration (section 3). In another test, the entire basin, including the strait east of 10.5° W, is deepened to 4615-m depth. In both experiments, the sea level of the Mediterranean Sea remains dominated by a uniform fluctuation that is coherent with the reference experiment but with amplitudes approximately

commensurate with the depth according to Eq. (4), further demonstrating the validity of this dynamic balance (Table 1).

Equation (4) is also consistent locally with the model sensitivity described in Fig. 11. For instance, Eq. (4) predicts a sensitivity of 3.7 cm in sea level change per 1 N m^{-2} coincident zonal wind stress within the strait at 35.5° N, 6° W (the depth and length of this model grid are 303 m and 111 km, respectively). Values in Fig. 11 away from the connecting region in the interior of either the Mediterranean or Atlantic basins do not necessarily match Eq. (4). This is because the balance does not strictly apply at these locations and because both ends of the sea level difference are either included or excluded in the definition of the basin average.

The dynamic balance described by Eqs. (2) and (4) is the well-known wind setup (e.g., Csanady 1982, p. 26) often established during strong wind events in lakes and coastal oceans. Typical occurrences of the wind setup concern the wind forcing over a relatively small region with the resulting sea level gradients across the domain. The novel aspect of the present situation is that the wind setup occurs over a relatively small region that connects two planetary-scale basins (the Mediterranean Sea and the rest of the global ocean) and that the sea level of each basin responds uniformly to this regional forcing.

The independence of the wind setup to the width of the forcing region in part explains why the present model has skill in simulating the observed basin-wide sea level fluctuation in spite of the model's coarse resolution. Equation (4) also represents a spatially integrated first-order balance over not only the Strait of Gibraltar but over the region connecting the Mediterranean Sea and the Atlantic Ocean. As discussed in the previous section, winds within the strait have the largest effect per unit area, but winds in the vicinity but outside the strait (e.g., the Alboran Sea and Atlantic Ocean immediately to the west of the strait) collectively account for as large a fraction of the basin-wide sea level variability as that within the strait (Fig. 13). The importance of such integrated effect also implies that small-scale processes, which may be important locally, may not be significant for the basin-mean sea level. For instance, the effects of strong wind events within the strait (e.g., Dorman et al. 1995) may be limited for the basin-mean sea level because of the relatively short spatial extent of the strait itself.

Last, Earth's rotation (Coriolis force) does not play a role in the dynamic balance of Eqs. (2) and (4). To test the effect of Earth's rotation, another barotropic experiment is conducted by setting the rotation rate to zero but with the topography the same as in the refer-

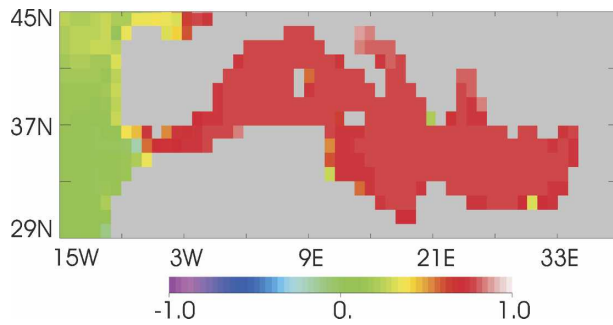


FIG. 16. Correlation between the sea levels of the wind-driven barotropic models with and without rotation.

ence experiment. Figure 16 shows the correlation between the sea level of this experiment and the same but with rotation. Although the sea level varies differently in the Atlantic Ocean because of rotational effects, that of the Mediterranean Sea is fairly similar between the two experiments. The sea level of the Mediterranean Sea is still dominated by the nearly uniform fluctuation but with values somewhat smaller than the reference calculation (Table 1). The difference in amplitude suggests that there are some parts of this oscillation that do depend on Earth's rotation (e.g., coastal Kelvin waves). Nevertheless, the result demonstrates that a significant fraction of the basin-wide sea level oscillation is indeed independent of Earth's rotational effects.

In a companion paper, Menemenlis et al. (2007) describe in more detail local physical processes responsible for establishing a dynamic balance between winds near Gibraltar Strait and Atlantic–Mediterranean sea level difference.

e. Comparison with atmospheric pressure effects

In the present study, as is common with other investigations, we have assumed an inverse barometer (IB) response in which the ocean adjusts isostatically to atmospheric pressure variations (Wunsch 1972). The IB assumption is generally accurate except for periods shorter than a few days where frictional effects in straits retard the response (Garrett and Majaess 1984; Candela 1991). However, recent observations also indicate a possible overisostatic variability at periods longer than 20 days where mean sea level changes of the Mediterranean Sea are larger than those inferred from an IB relationship (Le Traon and Gauzelin 1997). As is described below, however, such apparent deviations may in fact be partly due to the wind-driven fluctuation of the basin-mean sea level.

Figure 17a shows the first empirical orthogonal function of the nonseasonal component of IB sea level correction [i.e., how sea level would move isostatically to

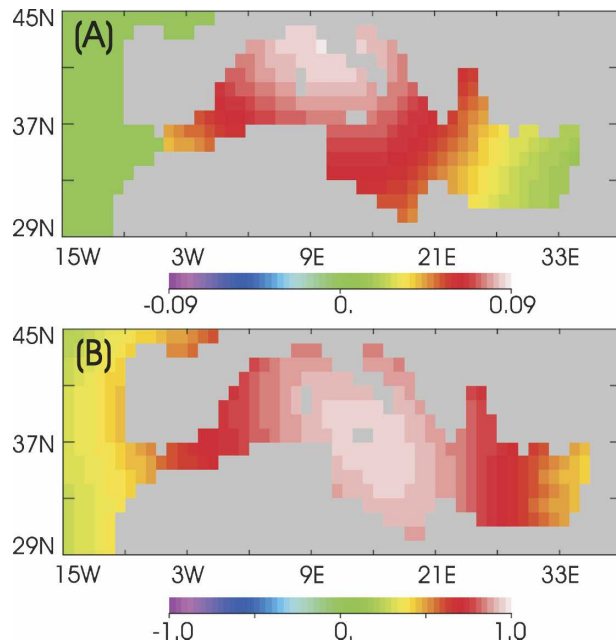


FIG. 17. Nonseasonal IB corrections: (a) first EOF over the Mediterranean Sea and (b) correlation with its basin mean. This first EOF accounts for 73% of the basin-wide variance of the nonseasonal atmospheric pressure correction. Significant spatial variabilities are found relative to similar modes and correlations of the observations (Figs. 3b and 5a) and model (Figs. 6b and 5b).

the pressure fluctuation and what has been removed from the altimetric observations (section 2)]. The EOF is based on 3-day averages of the 12-hourly surface pressure estimates of the NCEP–NCAR reanalyses. This first mode accounts for 73% of the nonseasonal variance of the correction and has the same sign across the basin. However, this mode has a larger-amplitude variation across the basin in comparison with equivalent EOFs of the altimeter data (Fig. 3b) and the model sea level (Fig. 5b). The correlation between its principal component and the basin-mean IB correction is 0.85, a value that is smaller than the corresponding correlations for the altimeter measurements (1.00) and model sea level (1.00). The smaller correlation indicates that the first EOF of the IB correction does not quite represent a basin-mean change as do those for the latter two. (The first EOF of the total IB correction is similar but is slightly more uniform across the basin and accounts for 71% of the correction's total variance.)

The correlation between the IB correction and its basin mean also reflects this modal structure (Fig. 17b). However, reflecting the correlation scale of atmospheric pressure systems, the significant correlation is seen to extend farther into the Atlantic Ocean than do those for altimetric measurements and the model sea level simulation (Fig. 5).

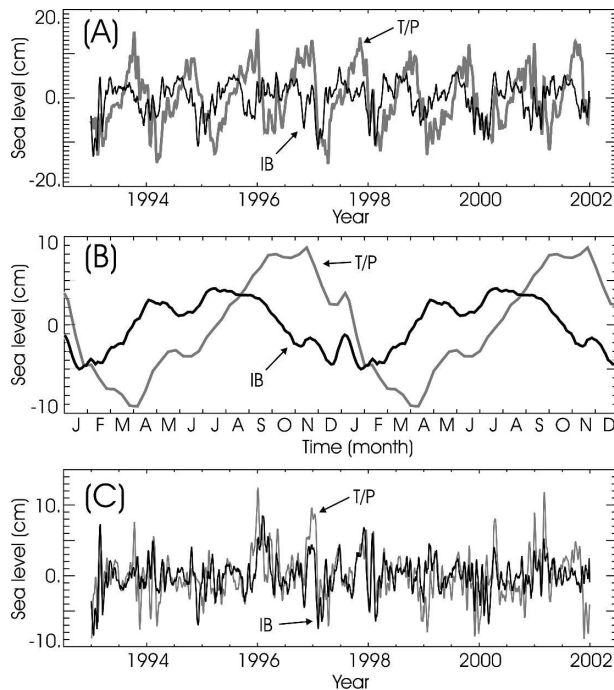


FIG. 18. Time series of basin-mean IB correction (black) and T/P sea level (gray): (a) total variability, (b) mean seasonal cycle, and (c) anomaly from the mean seasonal cycle. The 12-hourly IB correction is averaged with a 3-day running mean for clarity. The correlation coefficients between the two time series are 0.22, 0.09, and 0.43 in (a)–(c), respectively. The standard deviations of the IB corrections are 3.5, 2.9, and 2.2 cm in (a)–(c), respectively. In comparison, standard deviations of basin-mean T/P sea level are 6.5, 5.6, and 3.2 cm in (a)–(c), respectively. The T/P sea level is corrected for atmospheric pressure loading (see section 2).

Time series of the basin-mean IB sea level show changes having sizable variations similar to T/P sea level measurements (Fig. 18a). The two have standard deviations of 3.5 and 6.5 cm, respectively, based on 3-day-average sea level estimates. (The former has a standard deviation of 4.3 cm based on 12-hourly estimates.) The two time series are only marginally correlated (correlation coefficient is 0.22) in part because the average seasonal cycles of the two have different phases (Fig. 18b). The IB and T/P sea level are highest in July and November and are lowest in January and March, respectively.

Although the two seasonal cycles are out of phase with each other, the nonseasonal basin-mean components of the IB sea level and altimetric measurements are surprisingly coherent with comparable amplitudes (Fig. 18c), despite the fact that the IB corrections have already been applied to the latter measurements (section 2). The correlation coefficient between the two time series is 0.43.

The significant correlation between the IB correction

and the IB-corrected altimetric measurements suggests a possibly larger response of the Mediterranean Sea to atmospheric pressure variability than an isostatic balance (Le Traon and Gauzelin 1997). However, although Garrett (1983) postulated a pressure-driven resonance at periods shorter than 10 days (4 days for the whole basin), there is no obvious pressure-driven mechanism that could lead to such overisostatic variability at longer periods. A flow restriction at straits is generally expected to cause a smaller pressure-driven variability than an IB response. Instead, the apparent correlation between the IB correction and the altimetric measurements appears to reflect the correlation between atmospheric pressure and wind as opposed to a causal relationship between the pressure and the IB-corrected sea level.

Although the correlation between the nonseasonal IB correction and the sea level measurements is sizable (0.43), it is significantly lower than that between the wind-driven model simulation and the altimetric measurements (0.75; see Fig. 7). Spectral analysis also illustrates a closer agreement between the latter pair than the former (Fig. 8). For periods shorter than 20 days (0.05 cpd), the IB correction has significantly more variability than either the altimetric observations or the model. However, the IB correction is less coherent with the altimetric measurements than the model simulation is, especially at periods longer than 20 days (frequencies smaller than 0.05 cpd). At shorter periods, the IB correction has a significantly larger phase difference with altimetric measurements (IB leads by approximately 50°) than the model simulation has. These comparisons, in addition to differences in the spatial coherence discussed previously (Figs. 3, 6, and 17), show that the model's wind-driven response is able to explain the altimetric measurements better overall than possible residual pressure effects could.

Because the wind and atmospheric pressure are inherently correlated, a lack of correspondence between the IB correction and sea level may not necessarily be an indication of the ocean's departure from an inverse barometer response. For instance, Fu and Pihos (1994) describe apparent deviations from an IB response in the tropical Pacific due to remote wind forcing. Comparisons evidenced here suggest similar effects of wind-driven variability.

The wind-driven variability may also help explain the apparent in-phase correlation between the pressure in the western Mediterranean Sea and the current within the Strait of Gibraltar (Crépon 1965; see also Garrett 1983). Such a correlation at first is at odds with mass conservation. The current should be correlated with the

temporal change in the pressure instead, if the current is a response of the ocean to the pressure variations. However, the wind-driven fluxes would be in phase with the pressure fluctuations and may account for the observed phase relationship.

García Lafuente et al. (2002b) examined the flow through the Strait of Gibraltar and its relationship to pressure and wind forcing using current-meter observations in the strait and a numerical circulation model. Although pressure-driven variability dominates the exchange between the Mediterranean and Atlantic basins, wind-driven fluctuations are also found to play a significant role in the flux variations. In fact, on occasion, the wind-driven circulation is observed to dominate the flow through the strait (García Lafuente et al. 2002a). [See also Garrett et al. (1989).]

The relative magnitude of the model-simulated wind-driven transport through the Strait of Gibraltar and that expected from atmospheric pressure fluctuations are comparable to the results of García Lafuente et al. (2002b) and Garrett (1983). The net mass flux estimates through the strait and the corresponding basin-mean sea level fluctuations based on a 12-hourly IB sea level correction have standard deviations of 0.78 Sv and 1.3 cm, respectively, with maximum values of 3.34 Sv and 5.6 cm (April 1997). In comparison, equivalent transport and sea level variations based on the model's wind-driven fluctuation (using the model's sea level at 12-h intervals) have standard deviations of 0.22 Sv and 0.37 cm, with maximum values of 1.31 Sv and 2.19 cm (January 1994). Thus, on average, the wind-driven fluctuations of the basin-mean sea level and their associated flow through the strait are approximately one-third the magnitude of those driven by pressure, and are not negligible.

5. Summary and conclusions

Large-scale sea level fluctuations of the Mediterranean Sea are dominated by a variability that is nearly uniform in phase and amplitude over the entire basin. The nature of this basin-wide oscillation is studied using measurements from the TOPEX/Poseidon satellite altimeter and a numerical ocean circulation model.

At the annual period, the model's basin-wide sea level fluctuation is somewhat smaller than that of the observations and also has a slight difference in phase. This discrepancy may be due in part to the model's limited spatial resolution and its inaccurate representation of the effects of atmospheric and terrestrial freshwater fluxes. In the model, buoyancy forcing accounts for half the annual fluctuation of the basin-wide sea level. Most of this buoyancy-driven change is due to

seasonal heating and cooling. Wind forcing accounts for the remaining half of the mean annual fluctuation.

The buoyancy-driven and wind-driven annual components have different phases from each other. Atmospheric heating and cooling cause a nearly harmonic change in sea level over the course of a year with the highest sea level occurring in September and the lowest in March. In comparison, the wind-driven part of the annual cycle is somewhat skewed and irregular (i.e., nonharmonic), possibly because of the large interannual variability rendering the analyzed mean annual cycle nonrepresentative. The simulated wind-driven component has the highest sea level in December and the lowest in July. The sum of the buoyancy- and wind-driven sea level fluctuations is highest in December and lowest in March.

In contrast to the annual cycle, the model is fairly skillful in both amplitude and phase in simulating the nonannual component of the basin-wide fluctuation. This nonseasonal fluctuation is almost entirely wind driven.

Both the annual and nonannual components of the basin-wide wind-driven sea level fluctuation are largely barotropic changes of the basin that result from net mass flux anomalies through the Strait of Gibraltar. The mass flux is forced by winds in the strait and its neighboring region that connects the Mediterranean Sea and the Atlantic Ocean. This neighboring region includes the Alboran Sea and the Atlantic Ocean immediately to the west of the strait between the Iberian Peninsula and Africa.

A near-stationary dynamic balance is established between the wind stress and the sea level difference between the two basins connected by the strait (Figs. 11 and 13). This balance can be explained in part by wind setup in this connecting region [Eq. (2)]. The depth and length of the wind setup region, together with the along-strait wind stress, represent a form of control over the sea level difference between the two basins and, equivalently, the net volume transport through the strait [Eq. (4)]. In particular, to first approximation, the sea level difference between the two basins (and net transport through the strait) is proportional to the length of the wind setup region but inversely proportional to its depth and independent of its width.

Dynamically, the wind-driven sea level difference can be explained by the wind forcing, generating a net transport through the strait until a pressure difference develops between the two ends of the strait that balances the wind forcing. The sea surface pressure, or equivalently the sea level, within each basin connected by the strait responds uniformly to such net transport

anomalies, similar to the effects of atmospheric pressure forcing and of freshwater fluxes at the sea surface. The basin-wide wind-driven sea level fluctuation is reasonably well simulated by the model in spite of its limited resolution (1°). The model is skillful because the dynamic balance is an integral relationship over a large area; because the response is barotropic, independent of the ocean's stratification; and because the oscillation is independent of the width of the connecting region, in particular, the Strait of Gibraltar.

Although skillful overall, other remaining differences between the model and the altimetric measurements are notable and may indicate intrinsic inaccuracies in the model that may be due to its coarse resolution and/or incomplete physics. These differences include differences in the annual cycle noted above and spatial inhomogeneities. For instance, the altimetric observations show variations in the Adriatic and Aegean Seas that may be related to seiches and other local effects that are not simulated by the model. However, it should be noted that the basin-wide sea level fluctuation cannot be simulated by an isolated regional model of the Mediterranean Sea even if it is of high spatial resolution. This is because the wind-forced sea level fluctuation only determines the sea level difference and because the global mean sea level is time invariant (to first approximation). Therefore, the basin-wide fluctuation cannot be simulated with the correct amplitude without accounting for the relative size difference of the Mediterranean Sea and the rest of the global ocean.

The basin-wide wind-driven fluctuation is remarkable in that the sea level of an entire basin (Mediterranean Sea) is affected uniformly, and nearly instantaneously, by winds in the vicinity of (and its resulting ocean flux through) a strait. This is in stark contrast to the ocean's inverse barometer response in which the atmospheric pressure over the entire basin forces flow through the strait. The amplitude of this wind-driven sea level fluctuation can be as large as 10 cm and is comparable to changes associated with seasonal heating and cooling and the inverse barometer effect. Moreover, a sizable fraction of this variability occurs at intraannual time scales, occasionally changing amplitudes by more than 11 cm within 10 days. Some of the larger interannual variations in the basin-mean sea level are also due to this wind-driven variability.

The wind-driven basin-wide fluctuation may also help account for observed sea level variations near Gibraltar Strait. In particular, Garrett et al. (1990a,b) and others have hypothesized that observed sea level fluctuations near the strait reflect changes in the hydraulic state and consequently the baroclinic inflow and outflow through the strait. However, observations, such

as the depth of the interface between the inflowing Atlantic and outflowing Mediterranean water masses, are often out of phase with the observed sea level variability. Instead, wind-driven barotropic sea level fluctuations such as those described in the present study, which are independent of the hydraulic state, may help account for such discrepancies.

Other studies of sea level of the Mediterranean Sea may need to take into consideration the effects of such basin-wide fluctuations, in a way analogous to those of other environmental corrections such as those for tides and the inverse barometer effect. For instance, a significant fraction of the fast barotropic net mass change of the Mediterranean Sea could be otherwise aliased by satellite gravity measurements such as the Gravity Recovery and Climate Experiment (GRACE). There is also evidence of possible aliasing for altimetric observations such as TOPEX/Poseidon. The wind-driven fluctuations are also inherently correlated with the pressure-driven variability and contribute to the apparent deviation of the Mediterranean Sea from an inverse barometer response. The extent of such deviation warrants a reexamination in light of the wind-driven basin-wide fluctuation. Similar fluctuations may also be found in other semienclosed seas that are connected to larger basins (see, e.g., Ducet et al. 1999). These and other related subjects are left for future investigations.

Acknowledgments. The authors thank Lee-Lueng Fu, Roman Glazman, Harry Bryden, and Pierre-Yves Le Traon for their helpful suggestions. We are grateful to Srdjan Dobricic and another anonymous reviewer for their constructive comments on an earlier version of the manuscript. Benyang Tang and Benny Cheng carried out most of the numerical experiments. Victor Zlotnicki helped with the spectral analyses. This study is a contribution of the Estimating the Circulation and Climate of the Ocean (ECCO) Consortium, which is funded by the National Oceanographic Partnership Program. This research was carried out at the Jet Propulsion Laboratory (JPL), California Institute of Technology, under contract with the National Aeronautics and Space Administration.

A personal recollection in celebration of Prof. Carl Wunsch's 65th birthday by Ichiro Fukumori: As a tribute to Carl's accomplishments not only as a scientist but as an educator, I would like to share my fond memory of the following episode. Carl posed this question during my qualifying orals in graduate school: "Why did Stommel assume spatially *uniform* upwelling in his theory of abyssal circulation?" In answering, I discussed aspects of thermocline theory, how upwelling cold abyssal water was supposed to oppose down-

welling heat to form the thermocline, and how ubiquitous the thermocline is. Carl shook his head in disapproval and said, “That (answer) is not acceptable.” Neither were my other answers. Seeing that I was getting nowhere, Carl eventually provided this answer: “It’s because it was the *simplest*.” I was stunned. In one simple example, Carl taught me a fundamental approach in science. The incident was a defining moment in my early career, and the lesson has been my guiding principle ever since.

APPENDIX

The Model’s Adjoint Sensitivity to Forcing

A model’s adjoint provides an effective means to evaluate the sensitivity of a model’s state or its function to various model variables including forcing and parameters. In this study, the specific forcing responsible for the modeled basin-wide oscillation of the Mediterranean Sea is identified by analyzing the sensitivity of the model sea level to winds at various locations at different times using such an approach.

Specifically, we consider the sensitivity of the basin-averaged sea level of the Mediterranean Sea J at some time T ,

$$J(T) \equiv \int h(T) dS/S_{\text{Med}}, \quad (\text{A1})$$

where $h(T)$ is the model sea level at time T and the integration is carried out over the area S of the Mediterranean Sea, where S_{Med} is its total horizontal area.

The sensitivity of J to winds at an earlier instance can be evaluated using the model’s adjoint. Linearized about its simulated state, the model’s temporal evolution can be described by a linear equation (“tangent linear model”):

$$\mathbf{x}(t) = \mathbf{A}(t)\mathbf{x}(t-1) + \mathbf{G}(t)\mathbf{f}(t), \quad (\text{A2})$$

where $\mathbf{x}(t)$ is the model state vector at time t . Vector $\mathbf{f}(t)$ denotes prescribed, inhomogeneous variables of the linearized model and includes external forcing, in particular, winds. We denote column vectors and matrices as boldface lower- and uppercase variables, respectively. Matrices \mathbf{A} and \mathbf{G} denote the linearized model algorithm in matrix form. Matrix \mathbf{A} is the state transition matrix, and \mathbf{G} is the “forcing matrix” that relates the inhomogeneous variables to the model’s state.

Using the causal relationship between \mathbf{x} and \mathbf{f} [Eq. (A2)], the sensitivity of $J(T)$ to \mathbf{f} at some instance prior to T , say $T-N$, can be written, using the chain rule, as

$$\begin{aligned} \frac{\partial J(T)}{\partial \mathbf{f}(T-N)} &= \frac{\partial \mathbf{x}^T(T-N)}{\partial \mathbf{f}(T-N)} \frac{\partial \mathbf{x}^T(T-N+1)}{\partial \mathbf{x}(T-N)} \\ &\cdots \frac{\partial \mathbf{x}^T(T)}{\partial \mathbf{x}(T-1)} \frac{\partial J(T)}{\partial \mathbf{x}(T)}. \end{aligned} \quad (\text{A3})$$

Given Eq. (A2),

$$\frac{\partial \mathbf{x}^T(t)}{\partial \mathbf{f}(t)} = \mathbf{G}^T(t) \quad (\text{A4})$$

and

$$\frac{\partial \mathbf{x}^T(t)}{\partial \mathbf{x}(t-1)} = \mathbf{A}^T(t). \quad (\text{A5})$$

Then, Eq. (A3) can be written as

$$\frac{\partial J(T)}{\partial \mathbf{f}(T-N)} = \mathbf{G}^T(T-N) \mathbf{A}^T(T-N+1) \cdots \mathbf{A}^T(T) \frac{\partial J(T)}{\partial \mathbf{x}(T)}. \quad (\text{A6})$$

Matrix \mathbf{A}^T is the adjoint of \mathbf{A} and defines the adjoint of the model, Eq. (A2); namely,

$$\lambda(t-1) = \mathbf{A}^T(t)\lambda(t), \quad (\text{A7})$$

where λ is the adjoint state vector. The sensitivity of $J(T)$ to $\mathbf{f}(T-N)$ is therefore given by Eq. (A6) as an integration of the model adjoint backward in time from time T to $T-N$. [To minimize computational requirements, Eq. (A6) is evaluated from right to left as a series of adjoint model operations on a vector instead of left to right, which involves adjoint models operating on one another. In practice, the adjoint models (\mathbf{A}^T , \mathbf{G}^T) are implicit operators and are not explicit matrices.] The adjoint integration starts with the derivative of J with respect to the model state vector at time T , $\partial J(T)/\partial \mathbf{x}(T)$. (The mean model sea level is a diagnostic quantity of the state vector.) At time $T-N$, the resulting adjoint state vector is projected to the \mathbf{f} space by the adjoint of the “forcing matrix” operator \mathbf{G} . In particular, the sensitivity to wind is given by the corresponding elements of $\partial J(T)/\partial \mathbf{f}(T-N)$.

In the present study, we analyze the sensitivity of 10-day-averaged sea level to wind stress over the coincident and prior 10-day periods. The adjoint is derived using the automatic adjoint compiler the Transformation of Algorithms in FORTRAN (TAF, which is marketed by FastOpt; information online at www.FastOpt.com). The forward model and, consequently, its adjoint employ a 1-h time-stepping algorithm. Thus, the model code that implicitly prescribes operators \mathbf{A} and \mathbf{G} , and their adjoint, correspond to integrations over 1 h, and Eq. (A6) corresponds to the sensitivity of such 1-h-averaged variables.

The 10-day-averaged sensitivity is obtained by suitable averages of the sensitivities given by Eq. (A6). For instance, the sensitivity of the basin-mean sea level averaged between time $T - m$ and T (10-day interval),

$$\bar{J}(T) \equiv \sum_{i=0}^m J(T - i)/(m + 1), \quad (\text{A8})$$

to \mathbf{f} at time $T - N$ is given by

$$\begin{aligned} \frac{\partial \bar{J}(T)}{\partial \mathbf{f}(T - N)} &= \frac{1}{m + 1} \sum_{i=0}^m \frac{\partial J(T - i)}{\partial \mathbf{f}(T - N)} = \mathbf{G}^T(T - N) \mathbf{A}^T(T - N + 1) \cdots \mathbf{A}^T(T - m) \\ &\times \left\langle \frac{\partial J(T - m)}{\partial \mathbf{x}(T - m)} + \mathbf{A}^T(T - m + 1) \left\{ \frac{\partial J(T - m + 1)}{\partial \mathbf{x}(T - m + 1)} + \mathbf{A}^T(T - m + 2) \cdots \left[\frac{\partial J(T - 1)}{\partial \mathbf{x}(T - 1)} + \mathbf{A}^T(T) \cdot \frac{\partial J(T)}{\partial \mathbf{x}(T)} \right] \cdots \right\} \right\rangle / (m + 1). \end{aligned} \quad (\text{A9})$$

Alternatively, Eq. (A9) [and Eq. (A6)] can be written in a general form as

$$\frac{\partial \bar{J}(T)}{\partial \mathbf{f}(T - N)} = \frac{1}{m + 1} \mathbf{G}^T(T - N) \lambda(T - N), \quad (\text{A10})$$

where λ is governed by

$$\lambda(t - 1) = \mathbf{A}^T(t) \lambda(t) + \frac{\partial J(t - 1)}{\partial \mathbf{x}(t - 1)} H(t - 1). \quad (\text{A11})$$

Here,

$$\begin{aligned} H(t - 1) &= 1 \text{ when } T - m \leq t - 1 \leq T \\ &= 0 \text{ otherwise,} \end{aligned} \quad (\text{A12})$$

and the terminal condition is

$$\lambda(T + 1) = 0. \quad (\text{A13})$$

Last, because of linearity, the sensitivity of \bar{J} [Eq. (A8)] to the same \mathbf{f} over a 10-day interval between $t - N - m$ and $t - N$ (i.e., constant wind perturbation over 10 days) is given by

$$\sum_{i=0}^m \frac{\partial \bar{J}(T)}{\partial \mathbf{f}(T - N - i)} \equiv \frac{\partial \bar{J}(T)}{\partial \mathbf{f}_{10d}(T - N)}, \quad (\text{A14})$$

where $\mathbf{f}_{10d}(T - N)$ denotes the constant \mathbf{f} over the 10-day period ($T - N - m$ to $T - N$). Considering such sensitivity to 10-day fields \mathbf{f}_{10d} instead of every model time step reduces the number of temporal lags that the sensitivity needs to be saved at and thus significantly reduces the computational requirements of the analysis.

Then, given time series of \mathbf{f}_{10d} , and ignoring the effects of wind variabilities shorter than 10 days and longer than 360 days, \bar{J} can be estimated by

$$\bar{J}(T) \approx \sum_{N=0}^{360\text{days}} \mathbf{f}_{10d}^T(T - N) \frac{\partial \bar{J}(T)}{\partial \mathbf{f}_{10d}(T - N)}, \quad (\text{A15})$$

where the summation is performed at 10-day intervals (i.e., $N = 0, 10, 20$ days, ...). Assuming stationarity, Eq. (A14) can be written solely as a function of lag N such that

$$\frac{\partial \bar{J}(T)}{\partial \mathbf{f}_{10d}(T - N)} \equiv \bar{\mathbf{g}}(N). \quad (\text{A16})$$

Substituting Eq. (A16), Eq. (A15) can be recognized as a convolution:

$$\bar{J}(T) \approx \sum_{N=0}^{360\text{days}} \mathbf{f}_{10d}^T(T - N) \bar{\mathbf{g}}(N). \quad (\text{A17})$$

In particular, the sensitivity of $\bar{J}(T)$ to the 10-day constant wind $\tau_{10d}(i, j, t)$, where i, j, t denote model zonal and meridional indices and time, respectively, can be written as

$$\bar{J}(T) \approx \sum_{N=0}^{360\text{days}} \sum_{i,j} \tau_{10d}(i, j, T - N) \bar{g}(i, j, N), \quad (\text{A18})$$

where the vector inner product in Eq. (A17) has been explicitly expanded into an integration (sum) over the entire model domain (i, j). Here, $\bar{g}(i, j, N)$ denotes the particular elements of Eq. (A16) that correspond to the sensitivity of \bar{J} to a 10-day constant wind at spatial grid (i, j) at time lag N .

Equation (A18) can also be approximated using 10-day averages of wind, $\bar{\tau}$,

$$\bar{J}(T) \approx \sum_{N=0}^{360\text{days}} \sum_{i,j} \bar{\tau}(i, j, T - N) \bar{g}(i, j, N). \quad (\text{A19})$$

The differences between Eqs. (A18) and (A19), and the actual time series of \bar{J} , are due in part to fluctuations of the wind at time scales shorter than 10 days.

REFERENCES

- Arakawa, A., and V. R. Lamb, 1977: Computational design of the basic dynamical processes of the UCLA general circulation model. *General Circulation Models of the Atmosphere*, J. Chang, Ed., *Methods in Computational Physics*, Vol. 17, Academic Press, 173–265.
- Barnier, B., L. Siefridt, and P. Marchesiello, 1995: Thermal forcing for a global ocean circulation model using a three-year climatology of ECMWF analyses. *J. Mar. Syst.*, **6**, 363–380.
- Bormans, M., and C. Garrett, 1989: The effects of nonrectangular cross section, friction, and barotropic fluctuations on the exchange through the Strait of Gibraltar. *J. Phys. Oceanogr.*, **19**, 1543–1557.
- , —, and K. R. Thompson, 1986: Seasonal variability of the surface inflow through the Strait of Gibraltar. *Oceanol. Acta*, **9**, 403–414.
- Boyer, T. P., and S. Levitus, 1998: Objective analysis of temperature and salinity for the world ocean on a $1/4^\circ$ grid. NOAA NESDIS Atlas 11, 62 pp.
- Bryden, H. L., J. Candela, and T. H. Kinder, 1994: Exchange through the Strait of Gibraltar. *Progress in Oceanography*, Vol. 33, Pergamon, 201–248.
- Candela, J., 1991: The Gibraltar Strait and its role in the dynamics of the Mediterranean Sea. *Dyn. Atmos. Oceans*, **15**, 267–300.
- , 2001: Mediterranean Water and global circulation. *Ocean Circulation and Climate*, G. Siedler, J. Church, and J. Gould, Eds., Academic Press, 419–429.
- , C. D. Winant, and H. L. Bryden, 1989: Meteorologically forced subinertial flows through the Strait of Gibraltar. *J. Geophys. Res.*, **94**, 12 667–12 679.
- Cazenave, A., P. Bonnefond, F. Mercier, K. Dominh, and V. Toumazou, 2002: Sea level variations in the Mediterranean Sea and Black Sea from satellite altimetry and tide gauges. *Global Planet. Change*, **34**, 59–86.
- Crépon, M., 1965: Influence de la pression atmosphérique sur le niveau moyen de la Méditerranée Occidentale et sur le flux à travers le détroit de Gibraltar. *Cah. Océanogr.*, **17**, 15–32.
- Csanady, G. T., 1982: *Circulation in the Coastal Ocean*. D. Reidel, 279 pp.
- da Silva, A. M., C. C. Young, and S. Levitus, 1994: *Algorithms and Procedures*. Vol. 1, *Atlas of Surface Marine Data 1994*, NOAA Atlas NESDIS 6, 83 pp.
- Dickey, J. O., S. L. Marcus, O. de Viron, and I. Fukumori, 2002: Recent Earth oblateness variations: Unraveling climate and postglacial rebound effects. *Science*, **298**, 1975–1977.
- Dorman, C. E., R. C. Beardsley, and R. Limeburner, 1995: Winds in the Strait of Gibraltar. *Quart. J. Roy. Meteor. Soc.*, **121**, 1903–1921.
- Ducet, N., P. Y. Le Traon, and P. Gauzelin, 1999: Response of the Black Sea mean level to atmospheric pressure and wind forcing. *J. Mar. Syst.*, **22**, 311–327.
- Farmer, D. M., and L. Armi, 1986: Maximal two-layer exchange over a sill and through the combination of a sill and contraction with barotropic flow. *J. Fluid Mech.*, **164**, 53–76.
- Fu, L.-L., 2004: Latitudinal and frequency characteristics of the westward propagation of large-scale oceanic variability. *J. Phys. Oceanogr.*, **34**, 1907–1921.
- , and G. Pihos, 1994: Determining the response of sea level to atmospheric pressure forcing using TOPEX/Poseidon data. *J. Geophys. Res.*, **99**, 24 633–24 642.
- Fukumori, I., R. Raghunath, and L. Fu, 1998: Nature of global large-scale sea level variability in relation to atmospheric forcing: A modeling study. *J. Geophys. Res.*, **103**, 5493–5512.
- , T. Lee, B. Cheng, and D. Menemenlis, 2004: The origin, pathway, and destination of Niño-3 water estimated by a simulated passive tracer and its adjoint. *J. Phys. Oceanogr.*, **34**, 582–604.
- García Lafuente, J., J. Delgado, and F. Criado, 2002a: Inflow interruption by meteorological forcing in the Strait of Gibraltar. *Geophys. Res. Lett.*, **29**, 1914, doi:10.1029/2002GL015446.
- , E. A. Fanjul, J. M. Vargas, and A. W. Ratsimandresy, 2002b: Subinertial variability in the flow through the Strait of Gibraltar. *J. Geophys. Res.*, **107**, 3168, doi:10.1029/2001JC001104.
- Garrett, C., 1983: Variable sea level and strait flows in the Mediterranean: A theoretical study of the response to meteorological forcing. *Oceanol. Acta*, **6**, 79–87.
- , and F. Majaess, 1984: Nonisostatic response of sea level to atmospheric pressure in the eastern Mediterranean. *J. Phys. Oceanogr.*, **14**, 656–665.
- , J. Akerley, and K. Thompson, 1989: Low-frequency fluctuations in the Strait of Gibraltar from MEDALPEX sea level data. *J. Phys. Oceanogr.*, **19**, 1682–1696.
- , M. Bormans, and K. Thompson, 1990a: Is the exchange through the Strait of Gibraltar maximal or submaximal. *The Physical Oceanography of Sea Straits*, L. J. Pratt, Ed., Kluwer Academic, 271–294.
- , K. Thompson, and W. Blanchard, 1990b: Sea-level flips. *Science*, **348**, 292.
- Gent, P. R., and J. C. McWilliams, 1990: Isopycnal mixing in ocean circulation models. *J. Phys. Oceanogr.*, **20**, 150–155.
- Gross, R. S., I. Fukumori, and D. Menemenlis, 2003: Atmospheric and oceanic excitation of the Earth's wobbles during 1980–2000. *J. Geophys. Res.*, **108**, 2370, doi:10.1029/2002JB002143.
- , —, —, and P. Gegout, 2004: Atmospheric and oceanic excitation of length-of-day variations during 1980–2000. *J. Geophys. Res.*, **109**, B01406, doi:10.1029/2003JB002432.
- Junge, M. M., and T. W. N. Haine, 2001: Mechanisms of North Atlantic wintertime sea surface temperature anomalies. *J. Climate*, **14**, 4560–4572.
- Kalnay, E., and Coauthors, 1996: The NCEP/NCAR 40-Year Reanalysis Project. *Bull. Amer. Meteor. Soc.*, **77**, 437–471.
- Kim, S.-B., T. Lee, and I. Fukumori, 2004: The 1997–1999 abrupt change of the upper ocean temperature in the north central Pacific. *Geophys. Res. Lett.*, **31**, L22304, doi:10.1029/2004GL021142.
- Koopmans, L. H., 1974: *The Spectral Analysis of Time Series*. Academic Press, 366 pp.
- Korres, G., N. Pinardi, and A. Lascaratos, 2000: The ocean response to low-frequency interannual atmospheric variability in the Mediterranean Sea. Part I: Sensitivity experiments and energy analysis. *J. Climate*, **13**, 705–731.
- Large, W. G., J. C. McWilliams, and S. C. Doney, 1994: Oceanic vertical mixing: A review and a model with a nonlocal boundary-layer parameterization. *Rev. Geophys.*, **32**, 363–403.
- Larnicol, G., P.-Y. Le Traon, N. Ayoub, and P. De Mey, 1995: Mean sea level and surface circulation variability of the Mediterranean Sea from 2 years of TOPEX/Poseidon altimetry. *J. Geophys. Res.*, **100**, 25 163–25 177.

- Leder, N., and M. Orlić, 2004: Fundamental Adriatic seiche recorded by current meters. *Ann. Geophys.*, **22**, 1449–1469.
- Lee, T., and I. Fukumori, 2003: Interannual to decadal variation of tropical–subtropical exchange in the Pacific Ocean: Boundary versus interior pycnocline transports. *J. Climate*, **16**, 4022–4042.
- , —, D. Menemenlis, Z. Xing, and L.-L. Fu, 2002: Effects of the Indonesian Throughflow on the Pacific and Indian Oceans. *J. Phys. Oceanogr.*, **32**, 1404–1429.
- Le Traon, P.-Y., and P. Gauzelin, 1997: Response of the Mediterranean mean sea level to atmospheric pressure forcing. *J. Geophys. Res.*, **102**, 973–984.
- Marotzke, J., R. Giering, K. Q. Zhang, D. Stammer, C. Hill, and T. Lee, 1999: Construction of the adjoint MIT ocean general circulation model and application to Atlantic heat transport sensitivity. *J. Geophys. Res.*, **104**, 29 529–29 547.
- Marshall, J. C., A. Adcroft, C. Hill, L. Perelman, and C. Heisey, 1997: A finite-volume, incompressible Navier–Stokes model for studies of the ocean on parallel computers. *J. Geophys. Res.*, **102**, 5753–5766.
- Menemenlis, D., I. Fukumori, and T. Lee, 2007: Atlantic to Mediterranean sea level difference driven by winds near Gibraltar Strait. *J. Phys. Oceanogr.*, **37**, 359–376.
- NGDC, 1988: Digital relief of the surface of the Earth. Data Announcement 88-MGG-02, NOAA/National Geophysical Data Center, Boulder, CO.
- POEM Group, 1992: General circulation of the eastern Mediterranean. *Earth-Sci. Rev.*, **32**, 285–309.
- Ponte, R. M., D. A. Salstein, and R. D. Rosen, 1991: Sea level response to pressure forcing in a barotropic numerical model. *J. Phys. Oceanogr.*, **21**, 1043–1057.
- Ross, T., C. Garrett, and P.-Y. Le Traon, 2000: Western Mediterranean sea-level rise: Changing exchange flow through the Strait of Gibraltar. *Geophys. Res. Lett.*, **27**, 2949–2952.
- Send, U., and B. Baschek, 2001: Intensive shipboard observations of the flow through the Strait of Gibraltar. *J. Geophys. Res.*, **106**, 31 017–31 032.
- Stammer, D., C. Wunsch, I. Fukumori, and J. Marshall, 2002: State estimation in modern oceanographic research. *Eos, Trans. Amer. Geophys. Union*, **83**, 289, 294–295.
- Wang, O., I. Fukumori, T. Lee, and B. Cheng, 2004a: On the cause of eastern equatorial Pacific Ocean T–S variations associated with El Niño. *Geophys. Res. Lett.*, **31**, L15309, doi:10.1029/2004GL020188.
- , —, —, and G. Johnson, 2004b: Eastern equatorial Pacific Ocean T–S variations with El Niño. *Geophys. Res. Lett.*, **31**, L04305, doi:10.1029/2003GL019087.
- Wunsch, C., 1972: Bermuda sea level in relation to tides, weather, and baroclinic fluctuations. *Rev. Geophys. Space Phys.*, **10**, 1–49.